J Mater Sci (2011) 46:2557–2567
DOI 10.1007/s10853-010-5108-x

# Phase stabilities in molten Li/K carbonate of efficient matrix materials for molten carbonate fuel cells: thermodynamic calculations and experimental investigations

**Kailash Yashvant Patil · Sung Pil Yoon · Jonghee Han · Tae-Hoon Lim · Suk Woo Nam · In-Hwan Oh · Seong-Ahn Hong**

Received: 24 June 2010 / Accepted: 23 November 2010 / Published online: 16 December 2010


**Abstract** In this study, we investigated the thermodynamics and experimental performance of Al, Zr, and Ce species under anode and cathode gas conditions in Li/K carbonate at 650 °C. Among the Al, Zr, and Ce species investigated, we found that lithium aluminate ($LiAlO_2$), lithium zirconate ($Li_2ZrO_3$), and cerium/ceria oxide ($CeO_2$) were the most stable materials. Experimentally, we performed immersion tests in molten $(Li_{0.62}/K_{0.38})_2CO_3$ at 650 °C to evaluate the phase and microstructure stabilities of these materials. The $\gamma$-$LiAlO_2$ phase transformation, determined using X-ray diffractometry, was dependent on the immersion time. We performed similar measurements for $\alpha$-$LiAlO_2$, $Li_2ZrO_3$, and $CeO_2$ materials in molten Li/K carbonate at 650 °C. From immersion tests, the presence of the $\alpha$-$LiAlO_2$ phase revealed that phase transformation of $\gamma$-$LiAlO_2$ occurs in Li/K carbonate melts under cathode gas atmospheres; in contrast, no phase transformation was evident after immersion of the pure $\alpha$-$LiAlO_2$ phase in molten carbonate for 5,000 h. Furthermore, we found that $Li_2ZrO_3$ and $CeO_2$ were stable phases after immersion in molten carbonate at 650 °C, under both anode and cathode gas atmospheres, for more than 5,000 h.

K. Y. Patil · S. P. Yoon (✉) · J. Han · T.-H. Lim · S. W. Nam · I.-H. Oh · S.-A. Hong
Fuel Cell Research Center, Korea Institute of Science and Technology, 39-1 Hawolgok-Dong, Seongbuk-gu, Seoul 136-791, Republic of Korea
e-mail: spyoon@kist.re.kr

K. Y. Patil
School of Engineering, University of Science and Technology, Daejeon 305-333, Republic of Korea

## Introduction

Molten carbonate fuel cells (MCFCs) are stationary power systems that have attracted wide attention for commercialization worldwide. This technology provides fuel cell systems with an environmentally clean source of power generation in high efficiency and with pollution-free operation [1]. One of the key issues affecting the lifetime and durability of MCFCs is the thermodynamic stability of the components materials.

Lithium aluminate ($LiAlO_2$) is widely used as the matrix material in MCFCs because it has a relatively good susceptibility for retaining the electrolyte [2]. Extensive research has been undertaken toward the optimal design and preparation of $LiAlO_2$ in different shapes and sizes, which affect its corresponding properties and potential applications as the MCFC matrix. Nevertheless, $LiAlO_2$ undergoes allotropic transformations in molten carbonate at the MCFC operating temperature of 650 °C. Indeed, the poor phase stability, particle growth, increased pore size, and solubility of lithium aluminates under cell operation conditions can all decrease the MCFC service life (<40,000 h). Much attention has been paid recently to the study of $LiAlO_2$ materials that undergo the $\gamma$- to $\alpha$-phase transformation [3–5] and to the mechanism of particle growth, which originates through dissolution and precipitation under cell operating conditions [6–8]. A matrix featuring an increased median pore size and reduced electrolyte retention will lead to electrolyte loss, reactant cross-leakage, and ionic voltage loss and, thereby, degraded performance [9–11]. It is generally accepted that phase transformation of the $\gamma$-$LiAlO_2$ matrix occurs during cell operation at a temperature of 650 °C; this phase transformation influences the microstructures and properties of the matrix. It has been assumed that the

$\gamma$-$LiAlO_2$ phase is not thermodynamically stable in MCFC environments. To eliminate the structural and chemical weakness of using thermodynamically unstable electrolyte matrices, it remains of great interest to find new materials to improve or replace $\gamma$-$LiAlO_2$ as the matrix.

Thermodynamic studies are very applicable to investigations of the stability of molten carbonate melts and their component materials, to obtain information regarding the activity of oxygen and metal species. Thermochemical calculations have been employed to establish the electrochemical stability domains of Li–Na and Li–K carbonates at different temperature ranges under the anodic and cathodic conditions used in MCFCs [12]. Much effort has been exerted to obtain thermodynamic predictions of the stabilities of Ni, Ti, and Ce species in Li–Na and Li–K carbonates [13–16]. From thermodynamic studies, Chauvaut et al. [17, 18] reported a range of stabilities for molten alkali carbonates, mainly with regard to oxygen and metal species. Thermodynamic predictions on the stability of Ce species in molten alkali carbonate melt have been systematically developed under both oxidizing and reducing atmospheres. In all cases of Ce(IV), the $CeO_2$ form is a stable species found in molten carbonate conditions. Nevertheless, proving experimentally that $CeO_2$ is stable in both anode and cathode environments and also in Li–K molten carbonate at the operating temperature of 650 °C remains to be established. As a motivation for this current study, we noted that three species (Al, Zr, and Ce) contribute to the set of potentially thermodynamically stable matrix materials for MCFCs. There have, however, been almost no thermodynamic studies aimed at selecting Al and Zr species for use in molten carbonate. Very few data are available in thermochemical tables concerning Al and Zr compounds. In particular, no data are available for these materials in molten alkali carbonate at 650 °C. Indeed, for Al and Zr species, only the oxide, hydride, and carbide species are listed in thermochemical tables.

In this study, we performed thermodynamic calculations and experimental investigations into the applicability of using Al, Zr, and Ce species in MCFCs. We calculated the electrochemical and standard potentials of Al and Zr species and their products from reactions in Li–K melts at 650 °C using the thermodynamic predictions of Chauvaut et al. [17, 18] for Ti and Ce species. We then determined the phase transformations and stabilities and the microstructural behaviors of these lithiated/oxide compounds during immersion in Li/K carbonate at 650 °C under anodic and cathodic conditions. Herein, we discuss the phase and microstructural stabilities of the efficient matrix materials under various conditions.

## Thermodynamic formulations

The general properties and electrochemical stability domains of alkali molten carbonates have been fully analyzed in previous papers describing, in particular, the stability of oxygen species [12, 13], Ni [14, 15], and Ti [16] compounds. All the calculated potentials are referred to the $Li_2O/O_2$ system ($Li_2O$ being more stable than $K_2O$ in the mentioned eutectic) with values of $a$ ($Li_2O$) and $P$ ($O_2$) of 1 and 1 atm, respectively, with a standard potential $E^*(O_2/Li_2O)$ of 0 V. As much detail is available elsewhere [13, 16], it is unnecessary for us to discuss the concepts here. On the basis of thermodynamic calculations [19] and other data source [20, 21] available in the literature, the thermodynamic behavior of the Al, Zr, and Ce species in molten Li/K eutectic can be summarized under reducing and oxidizing atmospheres at 650 °C. The Al, Zr, and Ce species may exist in the melt under anodic and cathodic conditions in the forms of hydroxides, hydrides, and alkali and mixed oxides. Based on the thermodynamic parameters, the Nernst equations as a function of the activities of the compounds involved in the reactions, and the carbon dioxide partial pressure, we calculated the properties of these Al, Zr, and Ce species at 650 °C in MCFC environments.

## Example of the calculation for the $Al_2O_3/LiAlO_2$ system under anodic conditions

The thermodynamic reaction occurring in the melt is

$$Al_2O_3 + Li_2CO_3 + 2H_2O = 2LiAlO_2 + CO_2 + 2H_2 \quad (1)$$

The corresponding standard free enthalpies of reaction (1) can be calculated as follows:

$$\Delta_r G^\circ = 2\Delta_r G^\circ(LiAlO_2) + \Delta_r G^\circ(CO_2) - \Delta_r G^\circ(Al_2O_3) - \Delta_r G^\circ(Li_2CO_3) - 2\Delta_r G^\circ(H_2O), \quad (2)$$

where $\Delta_r G^\circ(LiAlO_2) = -1961.386$ kJ/mol at 650 °C, $\Delta_r G^\circ(CO_2) = -395.782$ kJ/mol at 650 °C, $\Delta_r G^\circ(Al_2O_3) = -1368.532$ kJ/mol at 650 °C, $\Delta_r G^\circ(Li_2CO_3) = 95.922$ kJ/kJ at 650 °C, and $\Delta_r G^\circ(H_2O) = -196.828$ kJ/mol at 650 °C.

We calculated, the standard potential of reaction (2) by using following equation:

$$E^\circ = \frac{\Delta_r G^\circ}{nF} \quad (3)$$

For anodic conditions, the corresponding Nernst equation is

$$E = E^{\circ} + 2.3\frac{RT}{2F}\left(\mathrm{pO}_2^{\frac{1}{2}} \times \frac{P_{\mathrm{H_2}}}{P_{\mathrm{H_2O}}}\right) + 2.3\frac{RT}{4F}\log(\mathrm{CO_2}) \quad (4)$$

Therefore, the electrochemical potential of reaction (2), determined using the Nernst equation, is

$$E = E^{\circ} + 2.3\frac{RT}{2F}\log\frac{a(\mathrm{LiAlO_2}) \times P(\mathrm{CO_2}) \times P(\mathrm{H_2})^2 \times P(\mathrm{O_2})}{a(\mathrm{Li_2CO_3}) \times a(\mathrm{Li_2O})^2 \times P(\mathrm{H_2O})^2}, \quad (5)$$

$$E = E^{\circ} + 2.3\frac{RT}{2F}(2\mathrm{p}K_{\mathrm{d}} * + 3\log P(\mathrm{CO_2})) + \frac{(\Delta_r G^{\circ})(\mathrm{H_2O})}{2F} + 2.3\frac{RT}{4F}\log\frac{a(\mathrm{LiAlO_2})}{a(\mathrm{Li_2CO_3})} \quad (6)$$

where $\Delta_r G^{\circ}(\mathrm{H_2O}) = 2.3RT\log\left[\left(P\mathrm{O}_2^{\frac{1}{2}} \times P\mathrm{H_2}\right)/P\mathrm{H_2O}\right]$. The cathodic conditions, the usual cathode atmosphere is constituted by a mixture of $CO_2$ (0.3 atm) and air (0.7 atm). In this case, the oxidizing agent is $O_2$.

Example of the calculation for the $Al_2O_3/LiAlO_2$ system under cathodic conditions

The thermodynamic reaction occurring in the melt is

$$\mathrm{Al_2O_3} + \mathrm{Li_2CO_3} + \frac{1}{3}\mathrm{O_2} = 2\mathrm{LiAlO_2} + \mathrm{CO_2} \quad (7)$$

The corresponding standard free enthalpies of reaction (7) can be calculated as follows:

$$\Delta_r G^{\circ} = 2\Delta_r G^{\circ}(\mathrm{LiAlO_2}) + \Delta_r G^{\circ}(\mathrm{CO_2}) - \Delta_r G^{\circ}(\mathrm{Al_2O_3}) - \Delta_r G^{\circ}(\mathrm{Li_2CO_3}) \quad (8)$$

Also, the standard potential of reaction (7) by using Eq. 3, and the following equation for cathodic conditions, the corresponding Nernst equation is

$$E = E^{\circ} - 2.3\frac{RT}{2F}\mathrm{pCO_2} + 2.3\frac{RT}{4F}\log(\mathrm{O_2}) \quad (9)$$

Therefore, the electrochemical potential of the reaction (7), obtained using the Nernst equation, is

$$E = E^{\circ} + 2.3\frac{RT}{2F}\mathrm{p}K_{\mathrm{d}} * + 2.3\frac{RT}{4F}\log\frac{a(\mathrm{LiAlO_2})}{a(\mathrm{Li_2CO_3})} + 2.3\frac{RT}{4F}\log P(\mathrm{CO_2}) \quad (10)$$

Tables 1, 2, 3 provide the electrochemical and standard potentials of selected Al, Zr, and Ce species, respectively, under anodic and cathodic conditions. For the Al, Zr, and Ce species, the anode gas atmospheres were calculated using values of $P(H_2/O_2/H_2O)$ of 0.8:0.001:0.12 and different values of $P(CO_2)$ (0.1, 0.01, 0.001, 0.0001); the cathode gas atmospheres were calculated using different values of $P(O_2)$ (0.1, 0.3, 0.5, 0.7) and $P(CO_2)$ (0.9, 0.7, 0.5, 0.3); see Figs. 1, 2, 3, respectively. Nernst equations under both anodic and cathodic conditions were established at 650 °C. According to thermodynamic calculations, when measuring the stability of species under anodic conditions, low electrochemical values ($E$) represent reducing

**Table 1** The detail values of the electrochemical and standard potentials of selected aluminum species in Li–K melts at 650 °C in anodic and cathodic conditions

| Species in anodic conditions | $E^{\circ}$ (V) | $E$ (V) (Li–K) | Species in cathodic conditions | $E^{\circ}$ (V) | $E$ (V) (Li–K) |
|---|---|---|---|---|---|
| AlC/$Al_2O$ | −3.2931 | −3.2611 | AlC/$Al_2O$ | −3.2931 | −1.2975 |
| AlC/$LiAlO_2$ | −2.0706 | −1.4716 | AlC/$LiAlO_2$ | −2.0706 | −1.1196 |
| $Al_2O$/$LiAlO_2$ | −1.6357 | −1.0367 | $Al_2O$/$LiAlO_2$ | −1.6357 | −0.6847 |
| $Al_2O_3$/$LiAlO_2$ | 0.4886 | 0.5501 | $Al_2O_3$/$LiAlO_2$ | 0.4886 | −0.6511 |
| $Li_2O$/$LiAlO_2$ | −0.3193 | 0.2796 | $Li_2O$/$LiAlO_2$ | −0.3193 | 0.6316 |
| $Al_2O$/$Al_2O_3$ | −3.1736 | −3.1416 | $Al_2O$/$Al_2O_3$ | −3.1736 | −2.7886 |

**Table 2** The detail values of the electrochemical and standard potentials of selected Zirconium species in Li–K melts at 650 °C in anodic and cathodic conditions

| Species in anodic conditions | $E^{\circ}$ (V) | $E$ (V) (Li–K) | Species in cathodic conditions | $E^{\circ}$ (V) | $E$ (V) (Li–K) |
|---|---|---|---|---|---|
| ZrC/ZrO | −0.6672 | −3.1887 | ZrC/ZrO | −0.6672 | −0.2822 |
| ZrC/$Li_2ZrO_3$ | −1.9244 | −1.3254 | ZrC/$Li_2ZrO_3$ | −1.9244 | −0.9734 |
| $ZrH_2$/ZrO | 0.2786 | 0.3105 | ZrH/ZrO | 0.2786 | 0.6635 |
| ZrO/$ZrO_2$ | −2.0595 | −2.0275 | ZrO/$ZrO_2$ | −2.0595 | −1.6745 |
| ZrO/$Li_2ZrO_3$ | −1.5908 | −0.9918 | ZrO/$Li_2ZrO_3$ | −1.5908 | −0.6398 |
| ZrC/$ZrH_2$ | −0.9458 | −0.9138 | ZrC/$ZrH_2$ | −0.9458 | −0.5608 |
| $ZrO_2$/$Li_2ZrO_3$ | −0.5611 | 0.0378 | $ZrO_2$/$Li_2ZrO_3$ | −0.5611 | 0.3898 |

**Table 3** The detail values of the electrochemical and standard potentials of selected Cerium species in Li–K melts at 650 °C in anodic and cathodic conditions

| Species in anodic conditions | $E^\circ$ (V) | $E$ (V) (Li–K) | Species in cathodic conditions | $E^\circ$ (V) | $E$ (V) (Li–K) | Ref. |
|---|---|---|---|---|---|---|
| $Ce/CeO_2$ | −2.322 | −2.3539 | $Ce/CeO_2$ | −2.322 | −1.9982 | [6] |
| $Ce/Ce_2O_3$ | −2.649 | −2.6809 | $Ce/Ce_2O_3$ | −2.649 | −2.3252 | [6] |

environments while high values represent oxidizing environments. For cathodic conditions, high electrochemical values represent oxidizing environments while low values represent reducing environments.

Our calculations suggested that $LiAlO_2$ would be the only stable Al species under the studied conditions. Moreover, in molten Li/K melts under anodic and cathodic conditions, metallic Al disproportionates into $Al_2O$ and $Al_2O_3$ species, which are not stable and are transformed into $LiAlO_2$, as indicated in Fig. 1a, b. Likewise, $Li_2ZrO_3$ would be the only stable Zr species under the studied conditions. Under both anodic and cathodic conditions, metallic Zr disproportionates into hydride, ZrO, and $ZrO_2$ species, which are not stable and are transformed into $Li_2ZrO_3$, as indicated in Fig. 2a, b. Also, $CeO_2$ would be the only stable Ce species under anodic and cathodic conditions, as indicated in Fig. 3a, b. Nevertheless, we required experimental evidence, by means of immersion tests, to confirm the thermodynamic stability of these species ($LiAlO_2$, $Li_2ZrO_3$, and $CeO_2$) in alkali carbonate melts at 650 °C.

## Materials and experimental procedures

Lithium aluminates (α-10 and γ-HAS-10 for $LiAlO_2$, Cyprus Foote, USA), lithium zirconate ($Li_2ZrO_3$, Alfa Aesar, USA), and cerium oxide ($CeO_2$, Alfa Aesar, USA) were tested in this present study. The physical properties of the as-received commercial materials are listed in Table 4. Eutectic mixtures of alkali metal carbonates (62 mol% $Li_2CO_3$/38 mol% $K_2CO_3$, anhydrous reagents; Junsei, Japan) were used. The phase and microstructures stabilities of these materials in molten $(Li_{0.62}/K_{0.38})_2CO_3$ melts were investigated under anode and cathode gas atmospheres through immersion tests. Figure 4 depicts the immersion tests, performed a using a home-built hot-pot system, at a temperature of 650 °C in an alumina crucible that contained the as-received powders in a mixture with molten $(Li_{0.62}/K_{0.38})_2CO_3$ melts. In these experiments, the anode atmosphere was a mixture of 72% $H_2$, 18% $CO_2$, and 10% $N_2$; the cathode atmosphere was a mixture of 33% $CO_2$ and 67% air. The gas was bubbled into the crucible at a flow rate of 10 mL/min. Under an anode or cathode gas

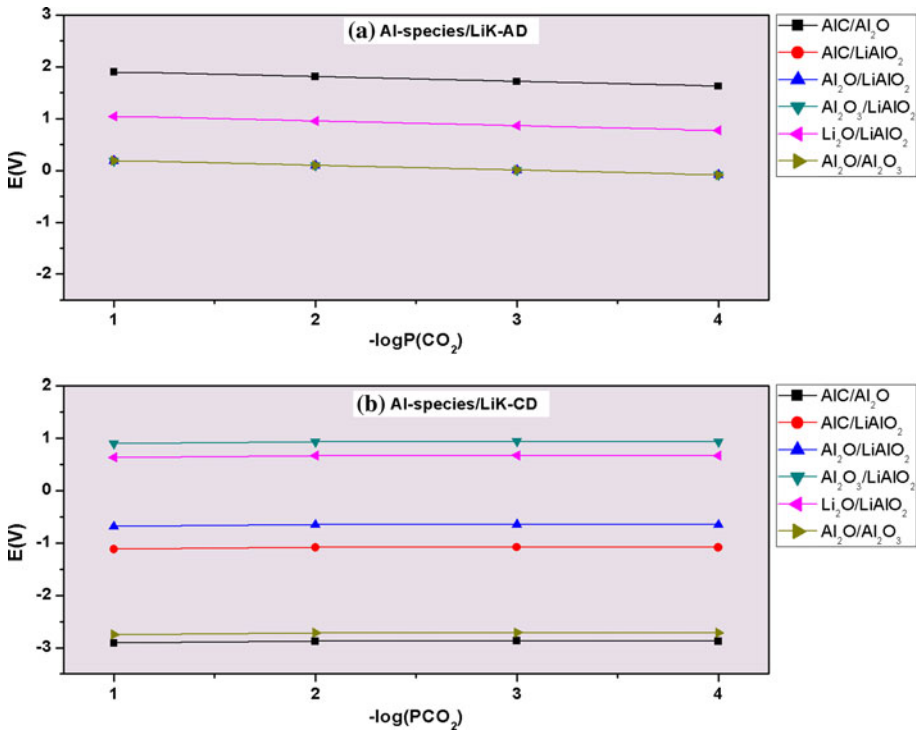


**Fig. 1** Electrochemical potential of Al species as function of different partial pressure of carbon dioxide in Li–K melts at 650 °C under **a** anodic conditions and **b** cathodic conditions

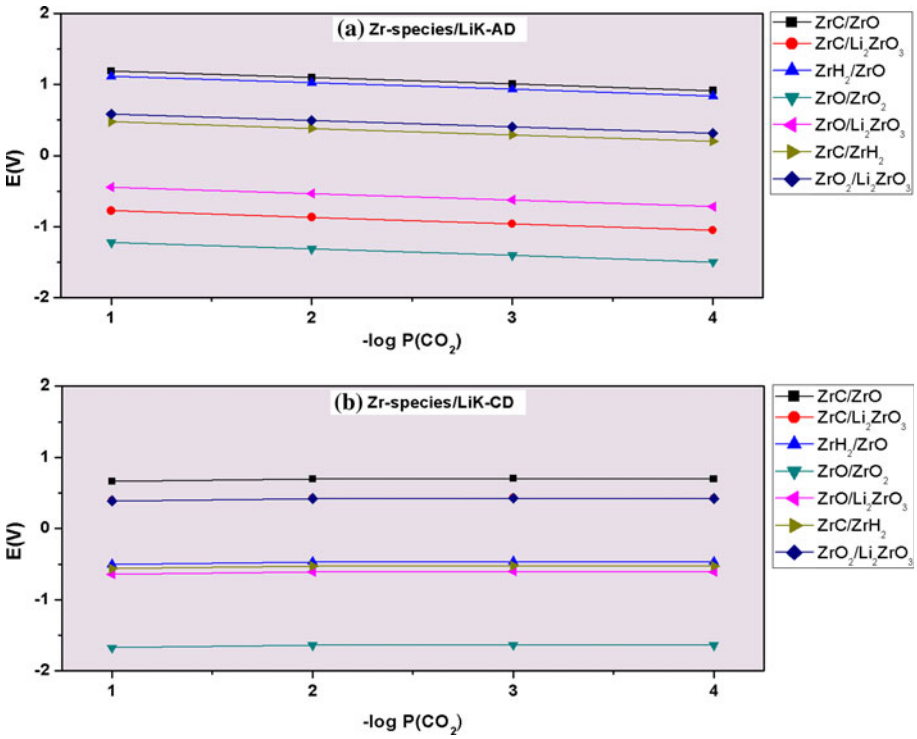


**Fig. 2** Electrochemical potential of Zr species as function of different partial pressure of carbon dioxide in Li–K melts at 650 °C under **a** anodic conditions and **b** cathodic conditions

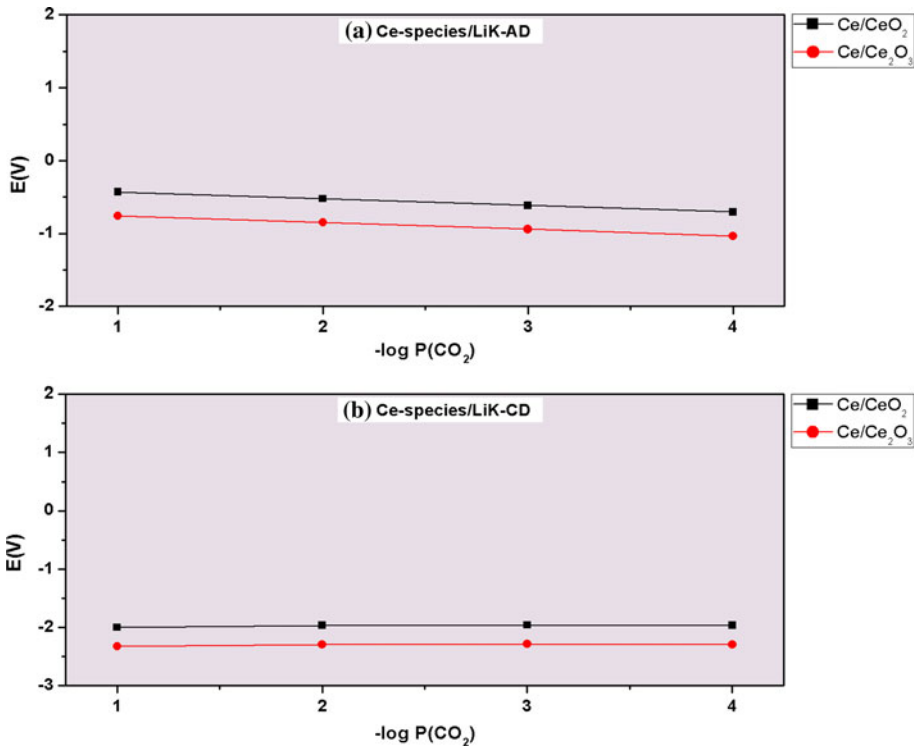


**Fig. 3** Electrochemical potential of Ce species as function of different partial pressure of carbon dioxide in Li–K melts at 650 °C under **a** anodic conditions and **b** cathodic conditions

environment, each immersion test was performed for a selected duration (>5,000 h). At the end of this time, to extract the carbonate melts, the powders were washed sequentially with mixture of glacial acetic acid and acetic anhydride and followed by ethanol wash dried in an oven, and then analyzed for textural and physical characterization. X-ray diffraction (XRD, Rigaku RINT-5200) and scanning electron microscopy (SEM, Philips XL30 ESEM) were used to identify the phases and microstructural stabilities, respectively, of the materials during exposure to

**Table 4** Physical properties of the as-received materials used in this work

| Materials | Crystalline phase | Average particle size (μm) | Specific surface area ($m^2\ g^{-1}$) |
|---|---|---|---|
| $\gamma$-$LiAlO_2$ | Tetragonal | 1 | 10 |
| $\alpha$-$LiAlO_2$ | Hexagonal | 1 | 10 |
| $Li_2ZrO_3$ | Monoclinic | 100 | 250 |
| $CeO_2$ | Cubic | 5 | 230 |

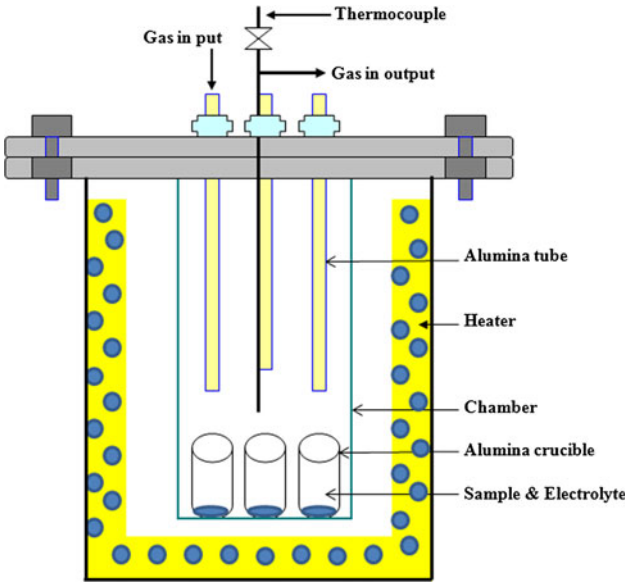


**Fig. 4** Schematic diagram of Hot-pot system for immersion test

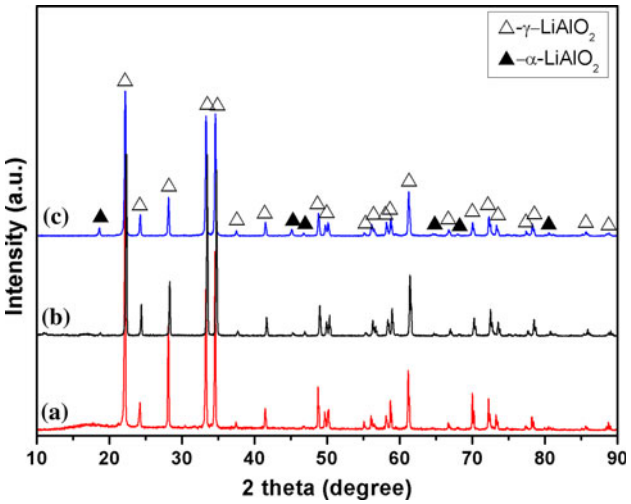


**Fig. 5** XRD patterns of $\gamma$-$LiAlO_2$ immersion in molten $(Li_{0.62}/K_{0.38})_2$ carbonate melts at 650 °C under cathode gas atmospheres, (a) initial, (b) 2,000, and (c) 5,000 h duration

Li/K carbonate melts under MCFC conditions. The surface areas of these materials were measured using BET equipment (Gemini 2375, Micromeritics, USA).

## Results and discussion

### Phase stability

First, we investigated the influence of molten Li/K carbonate at 650 °C on the phase stabilities of the as-received powders. Figure 5 compares the XRD patterns of the as-received $\gamma$-$LiAlO_2$ powder and after the sample obtained after immersion in molten carbonate at 650 °C under cathode gas atmospheres for 2,000 and 5,000 h. We observe the crystalline phase of $\alpha$-$LiAlO_2$, revealing that the $\gamma$-$LiAlO_2$ phase transformation occurred in molten carbonate at 650 °C under cathode gas atmospheres. The $\alpha$-$LiAlO_2$ phase appeared after performing the immersion test for 2,000 h (Fig. 5b) and was much better defined after 5,000 h (Fig. 5c). Notably, the diffraction peaks of the $\gamma$-phase narrowed and their intensity decreased greatly after an immersion time of 2,000 h. Increasing the immersion time to 5,000 h caused the intensity of the $\alpha$-$LiAlO_2$ peaks to increase at the expense of those of $\gamma$-$LiAlO_2$. Thus, the formation of the $\alpha$-$LiAlO_2$ phase accelerated upon increasing the immersion time. Thus, we conclude that the $\gamma$-$LiAlO_2$ phase transformation occurred during the 5,000-h immersion test under cathode gas atmospheres.

Figure 6 displays XRD patterns of the as-received $\alpha$-$LiAlO_2$ and the sample obtained after immersion in molten carbonate at 650 °C under cathode gas atmosphere. We found that the $\alpha$-$LiAlO_2$ phase was stable in molten Li/K carbonate during this immersion test performed for 2,000 h (Fig. 6b) and did not transform to any other phase, even after 5,000 h (Fig. 6c). Thus, no reversible phase transformation occurred during these immersion tests. Thus, the crystalline phase of $\alpha$-$LiAlO_2$ is stable and remains unchanged during the 5,000-h immersion test. In several studies, $LiAlO_2$ has been observed to transform into the $\gamma$-phase, followed by growth of a new $\alpha$-phase [3–7]. In this study, we also observed transformation of the $\gamma$-$LiAlO_2$ phase. The rate of transformation of $LiAlO_2$ phases depends on the immersion time in Li/K melts as well as the gas atmosphere and temperature. It has been assumed that the $\gamma$-phase is stable at high temperatures (>650 °C) under low partial pressures of $CO_2$ and that the $\alpha$-phase is stable at low temperatures (≤650 °C) under high partial pressures

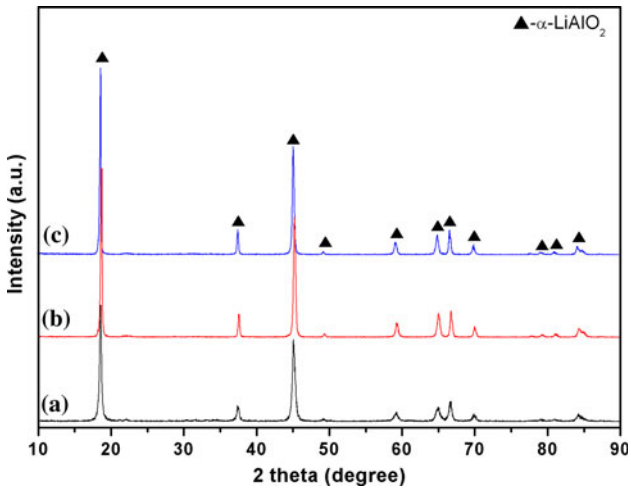


**Fig. 6** XRD patterns of α-$LiAlO_2$ immersion in molten $(Li_{0.62}/K_{0.38})_2$ carbonate melts at 650 °C under cathode gas atmospheres, (a) initial, (b) 2,000, and (c) 5,000 h duration

of $CO_2$ [22–25]. During the immersion process, the transformation of the γ-phase to the α-phase becomes the rate-determining step and, therefore, the temperature has a significant impact. Nevertheless, we have found that the α-to-γ phase transformation does not occur at 650 °C under an atmosphere of 30% $CO_2$ and 70% air.

Figure 7 shows XRD patterns of the as-received $Li_2ZrO_3$ powder and the samples obtained after immersion in molten $(Li_{0.62}/K_{0.38})_2CO_3$ melts at 650 °C for different periods of time under anode (Fig. 7a) and cathode (Fig. 7b) gas atmospheres. All of the peaks correspond to the crystalline monoclinic phase of $Li_2ZrO_3$ (JCPDS-ICDD PDF-2 # 33-0843), with the intensities matching those of the powder diffraction data very well. We observe no evidence for the formation of other phases in the molten carbonate under either gas atmosphere for the immersion tests performed for up to 5,000 h duration. Thus, we conclude that undergoes no chemical reactions with molten Li–K carbonate melts not structural change under reducing or oxidizing atmospheres. Indeed, $Li_2ZrO_3$ remained in its original monoclinic phase with no substantial change in weight after immersion for over 5,000 h.

Figure 8 shows XRD patterns of the as-received $CeO_2$ powders and the samples obtained after immersion in molten $(Li_{0.62}/K_{0.38})_2CO_3$ melts at 650 °C for different lengths of time under anode and cathode gas atmospheres. All of the peaks correspond to those of the cubic crystalline phase of $CeO_2$ (JCPDS-ICDD PDF-2 # 43-802); the signal intensities match those of the powder diffraction data very well. We observed no evidence of any reactions between $CeO_2$ and the molten carbonate at 650 °C under MCFC conditions in immersion tests performed for up to 5,000 h; indeed, only the peaks of $CeO_2$ were present. Thus, we conclude that no reduction phenomena occurred for the $CeO_2$ particles exposed to the molten carbonate under the reducing atmosphere during the 5,000-h immersion test; similarly, we conclude that no other oxide formed from $CeO_2$ under the oxidizing atmospheres during the 5,000-h immersion test.

## Microstructural behavior

We used SEM to characterize the surface morphologies of the as-received materials before and after their immersion in Li/K at 650 °C. Figure 9 shows the surface

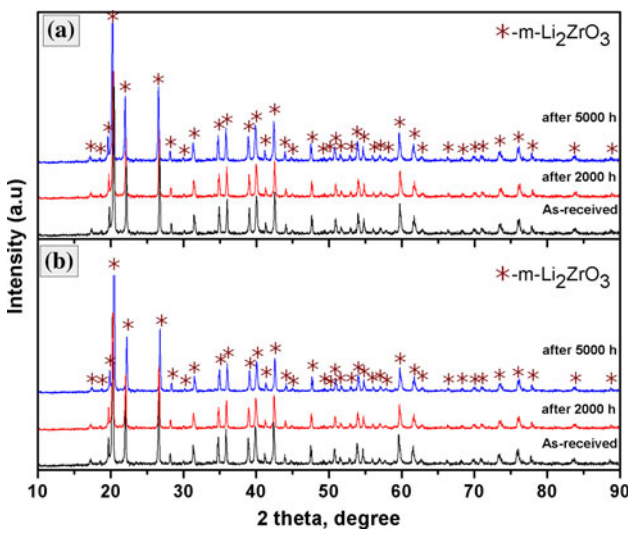


**Fig. 7** XRD patterns of $Li_2ZrO_3$ material immersion in molten $(Li_{0.62}/K_{0.38})_2$ carbonate melts at 650 °C under (a) anodic conditions after 2,000 and 5,000 h duration; (b) cathodic conditions after 2,000 and 5,000 h duration

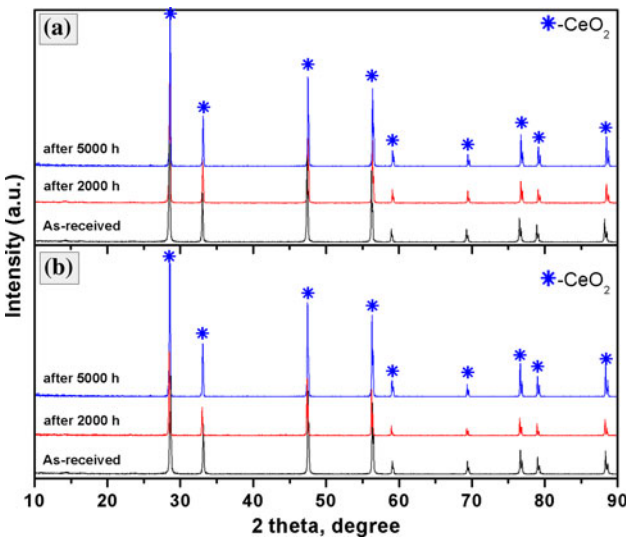


**Fig. 8** XRD patterns of $CeO_2$ material immersion in molten $(Li_{0.62}/K_{0.38})_2$ carbonate melts at 650 °C under (a) anodic conditions after 2,000 and 5,000 h duration; (b) cathodic conditions after 2,000 and 5,000 h duration

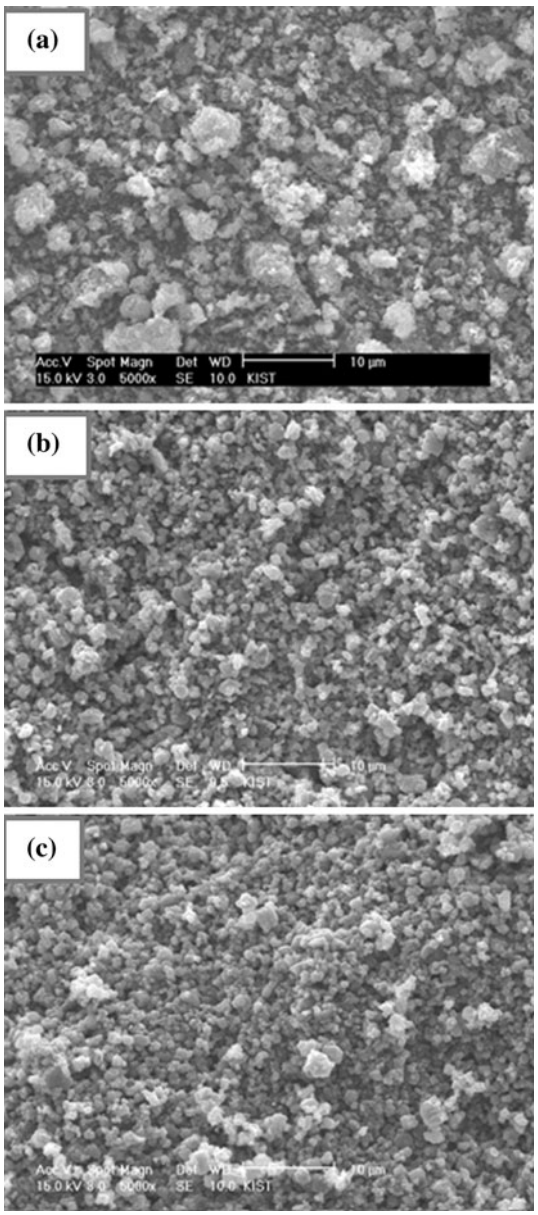


**Fig. 9** Surface morphology of $\gamma$-$LiAlO_2$ immersion in molten $(Li_{0.62}/K_{0.38})_2$ carbonate melts at 650 °C under cathode gas atmospheres, (**a**) initial, (**b**) 2,000, and (**c**) 5,000 h duration

morphologies of the $\gamma$-$LiAlO_2$ powder after immersion in molten carbonate under the cathode gas atmosphere for up to 5,000 h. The SEM images reveal that the $\gamma$-$LiAlO_2$ surface became smoother upon increasing the immersion time, compared with that of the as-received powder (Fig. 9a). An immersion time of only 2,000 h had a considerable influence on the microstructure evolution. The morphology of the $\gamma$-$LiAlO_2$ powder indicates that the particle growth occurred mainly as a result of a transformation process during the 2,000-h immersion test (Fig. 9b). The grain size of $\gamma$-$LiAlO_2$ increased slightly upon prolonging the immersion time up to 5,000 h (Fig. 9c). Notably, this kind of $\gamma$-$LiAlO_2$ particle growth is associated with a transformation that results in a decrease in the specific surface area (Table 5). Such a morphological transformation occurring for $\gamma$-$LiAlO_2$ powder in a hot-pot system suggests that similar results would also be expected in MCFC single cell/stack systems.

The microstructure of $\alpha$-$LiAlO_2$ prior to the test was almost same as that of $LiAlO_2$. Figure 10b indicates that the particles were well defined and no significant change in the particle/grain size occurred after performing the immersion test for 2,000 h. Indeed, the $\alpha$-$LiAlO_2$ particle size remained constant and the microstructure do not change upon extending the immersion test duration up to 5,000 h (Fig. 10c). We did, however, observe a decreasing in surface area when the immersion test was performed for more than 5,000 h (Table 5). Consequently, we consider $\alpha$-$LiAlO_2$ to be stable in molten carbonate because its crystalline phase and microstructure did not change during the 5,000-h immersion test.

Figures 11 and 12 display the microstructural behavior of the $Li_2ZrO_3$ material after immersion in molten $(Li_{0.62}/K_{0.38})_2CO_3$ melts at 650 °C under the anode and cathode gas atmospheres, respectively. The average size of the as-received particles was 100 μm. The particle size remained constant and the microstructure did not change when these immersion tests were performed for more than 5,000 h under either atmosphere, suggesting the existence of a monoclinic structure. Indeed, the SEM images of $Li_2ZrO_3$ samples obtained after immersion for 5,000 h were very close to those of the initial powder. The surface area of the monoclinic $Li_2ZrO_3$ decreased slightly to a constant value ($250\ m^2\ g^{-1}$) after we performed the immersion test for 5,000 h (Table 5). The tendency of the surface area to change slightly indicates that particle size growth was not accelerated during the immersion process under either the anode and cathode gas atmospheres. Thus, monoclinic $Li_2ZrO_3$ maintained its specific surface area in molten Li/K carbonate; we expect it to exhibit an excellent stability and morphology under MCFC conditions.

Figure 13 displays the surface morphologies of the $CeO_2$ powder exposed to the carbonate melt under anode gas conditions. The surface of the pure $CeO_2$ sample became smoother, along with particle growth, during the first 2,000 h of the immersion test (Fig. 13b); immersion for 5,000 h caused the $CeO_2$ particle size to increase further (Fig. 13c). Figure 14 shows the surface morphologies of the $CeO_2$ sample after immersion in molten carbonate under the cathode gas atmosphere. After 2,000 h (Fig. 14b), the size of the $CeO_2$ particles had begun to increase; after 5,000 h of immersion (Fig. 14c), they had almost doubled in size. The growth of the $CeO_2$ particles was, however, faster in Li/K carbonate melt under the anode gas atmosphere than under the cathode

**Table 5** Specific surface area of as-received materials exposure in molten carbonate at 650 °C

| Materials | Surface area ($m^2\ g^{-1}$) in MCFC environments | | | | |
|---|---|---|---|---|---|
| | Oxidizing atmospheres ($CO_2$/air) | | | Reducing atmospheres ($H_2/CO_2/N_2$) | |
| | Initial | After 2,000 h | After 5,000 h | After 2,000 h | After 5,000 h |
| $\gamma$-$LiAlO_2$ | 10 | 5.10 | 2.8 | – | – |
| $\alpha$-$LiAlO_2$ | 10 | 4.35 | 1.10 | – | – |
| $Li_2ZrO_3$ | 250 | 245 | 243 | 241 | 238 |
| $CeO_2$ | 230 | 217.3 | 192.4 | 196.3 | 180.6 |

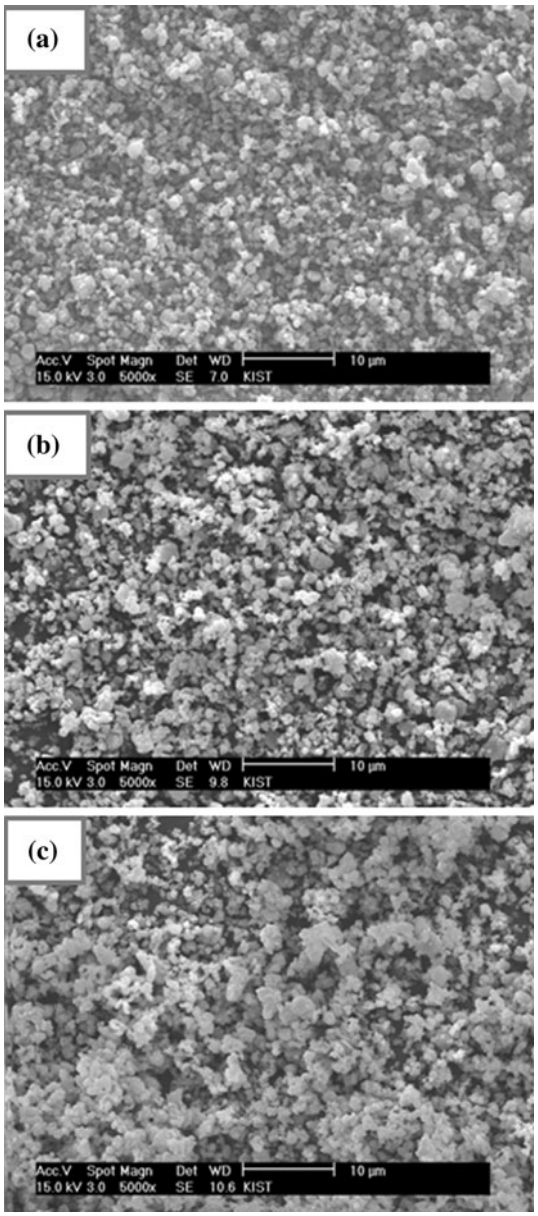


**Fig. 10** Surface morphology of $\alpha$-$LiAlO_2$ immersion in molten $(Li_{0.62}/K_{0.38})_2$ carbonate melts at 650 °C under cathode gas atmospheres, (**a**) initial, (**b**) 2,000, and (**c**) 5,000 h duration

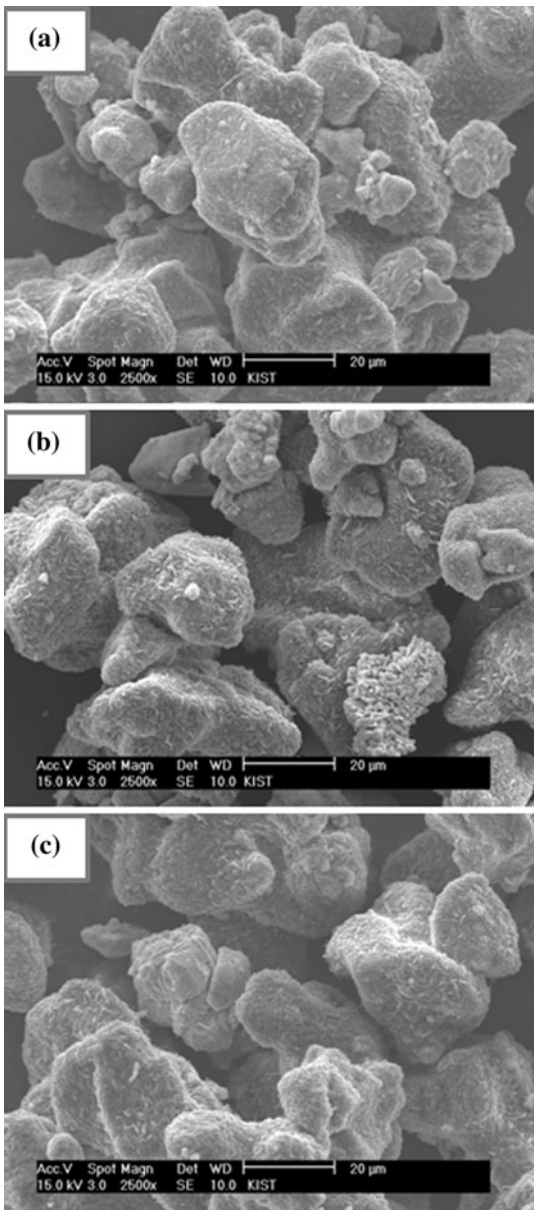


**Fig. 11** Surface morphology of $Li_2ZrO_3$ immersion in molten $(Li_{0.62}/K_{0.38})_2$ carbonate melts at 650 °C under anode gas atmospheres, (**a**) initial, (**b**) 2,000, and (**c**) 5,000 h duration

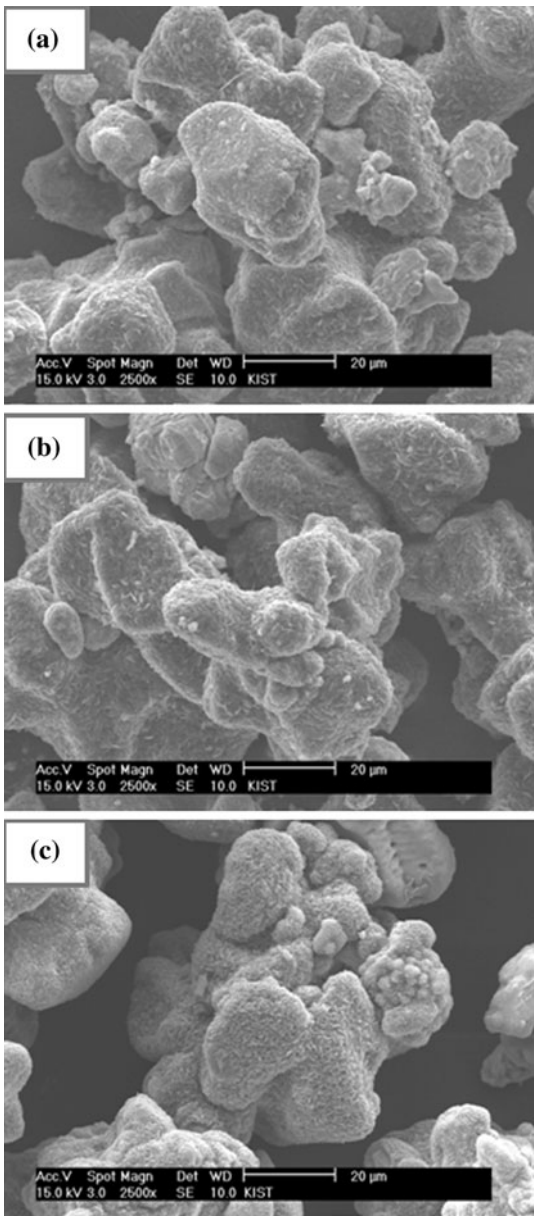


**Fig. 12** Surface morphology of $Li_2ZrO_3$ immersion in molten $(Li_{0.62}/K_{0.38})_2$ carbonate melts at 650 °C under cathode gas atmospheres, (**a**) initial, (**b**) 2,000, and (**c**) 5,000 h duration

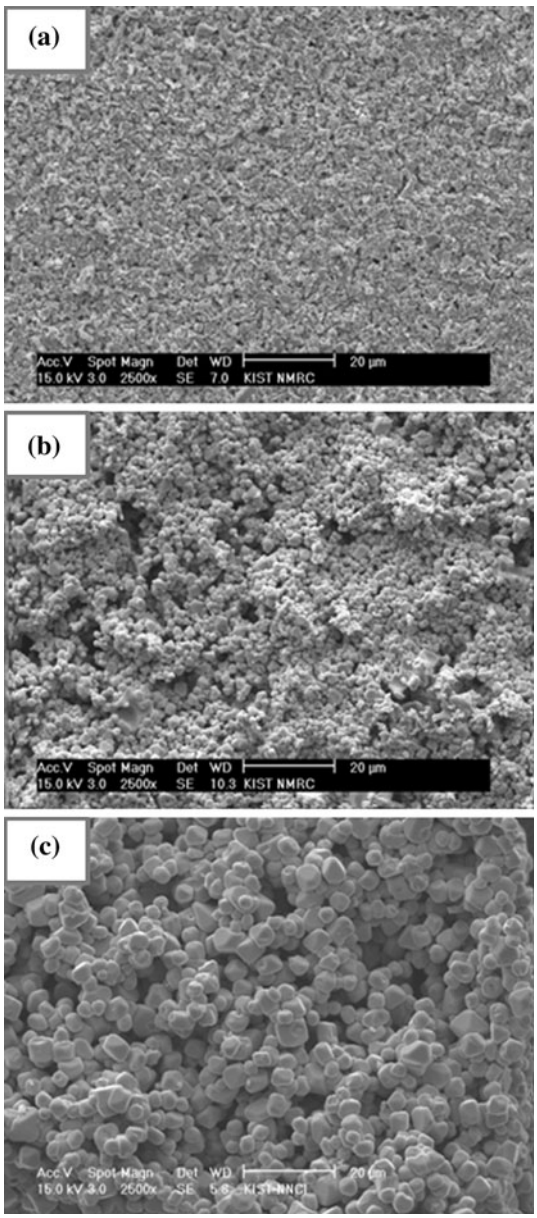


**Fig. 13** Surface morphology of $CeO_2$ immersion in molten $(Li_{0.62}/K_{0.38})_2$ carbonate melts at 650 °C under anode gas atmospheres, (**a**) initial, (**b**) 2,000, and (**c**) 5,000 h duration

gas atmosphere. We believe that the pure $CeO_2$ particle growth was due to the liquid phase sintering process during exposure to the molten carbonate at 650 °C. The tendency of the surface area to decrease (Table 5) also indicates that particle growth of $CeO_2$ occurred under both anode and cathode conditions. The rate of decrease of the surface area of the $CeO_2$ particles was faster under the anode gas conditions than it was under the cathode gas conditions.

## Conclusions

In this study, we investigated the phase behavior and microstructural stabilities of various materials when subjected to molten Li/K carbonate. In addition, we determined the effects of the gas atmosphere on the growth and phase transformations of these particles during immersion tests. We observed accelerated transformation and particle growth of $\gamma$-$LiAlO_2$ in Li/K melts at 650 °C under typical cathode gas atmospheres for immersion tests performed for up to 5,000 h. In contrast, the $\alpha$-$LiAlO_2$ phase did not

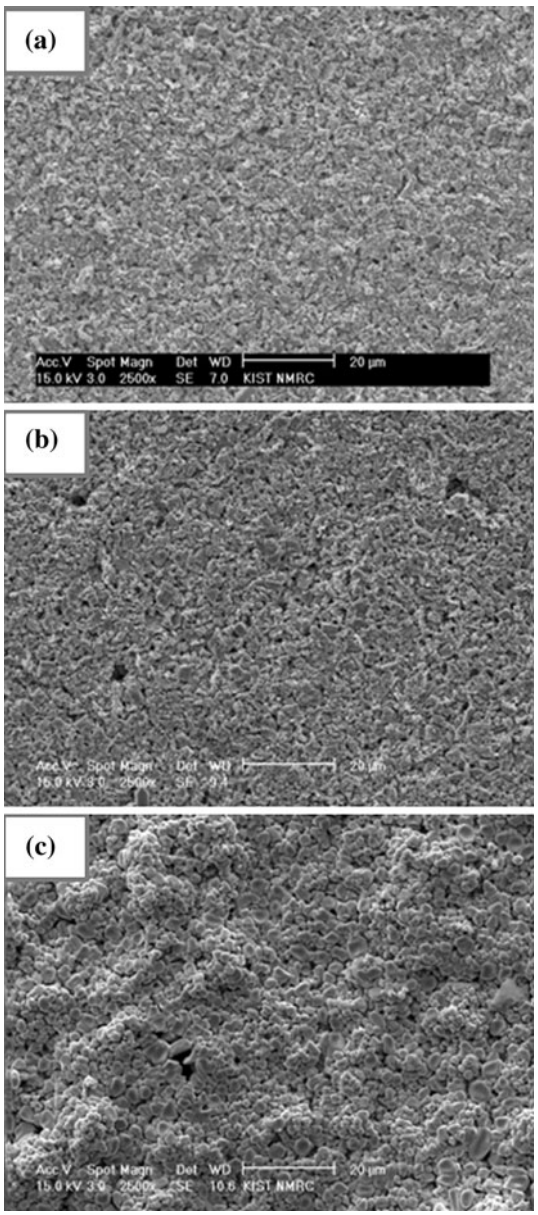


**Fig. 14** Surface morphology of $CeO_2$ immersion in molten $(Li_{0.62}/K_{0.38})_2$ carbonate melts at 650 °C under cathode gas atmospheres, (**a**) initial, (**b**) 2,000, and (**c**) 5,000 h duration

undergo transformation to the $\gamma$-$LiAlO_2$ phase in Li/K melts at 650 °C during immersion tests performed for up to 5,000 h. Phase stability studies revealed that the $\alpha$-$LiAlO_2$ phase is more stable than the $\gamma$-$LiAlO_2$ phase at 650 °C when immersed in the molten carbonate for more than 5,000 h. The phases and microstructures of $Li_2ZrO_3$ and $CeO_2$ materials remained unchanged after immersion in molten $(Li_{0.62}/K_{0.38})_2CO_3$ melts at 650 °C under typical MCFC environments (anode or cathode gas conditions). XRD patterns revealed the phase stability of both $Li_2ZrO_3$ and $CeO_2$ in $(Li_{0.62}/K_{0.38})_2CO_3$ melts; we observed no evidence for phase transformations or secondary phases under either anode or cathode gas conditions when we performed the immersion tests for durations of more than 5,000 h. Thus, $Li_2ZrO_3$ and $CeO_2$ materials appear to be chemically stable under MCFC environments. In the $CeO_2$ immersion test, the main influence on the microstructure was that the rate of particle growth was faster under the anode gas conditions than under the cathode gas conditions.

**Acknowledgement** This study was supported financially by the Fuel Cell Research program of the Korea Institute of Science and Technology.

## References

1. Maru HC, Farooque M, Pigeaud A (1990) In: Proceedings of the second symposium on MCFC technology, The Electrochemical Society, Pennington, NJ, p 121
2. Finn PA (1980) J Electrochem Soc 127:236
3. Terada S, Nagashima I, Higaki K, Ito Y (1998) J Power Sources 75:223
4. Terada S, Higaki K, Nagashima I, Ito Y (1999) J Power Sources 83:227
5. Tanimoto K, Yanagida M, Kojima T, Tamiya Y, Matsumoto H, Miyazaki Y (1998) J Power Sources 72:77
6. Sotouchi H, Watanabe Y, Kobayashi T, Murai M (1992) J Electrochem Soc 139(4):1127
7. Murai M, Takizawa K, Soejima K, Sotouchi H (1996) J Electrochem Soc 143(9):2776
8. Takizawa K, Hagiwara A (2002) J Power Sources 89:127
9. Fairchild GH, Brown PM (1986) In: Proceedings of the fuel cell seminar, Tucson, AZ, p 239
10. Ribeiro RA, Silva GG, Mohallem NDS (2001) J Phys Chem Solids 62:857
11. Tomimatsu N, Ohzu H, Akasaka Y, Nakagawa K (1997) J Electrochem Soc 144:4182
12. Moutiers G, Cassir M, Devynck J (1992) J Electroanal Chem 324:175
13. Cassir M, Moutiers G, Devynck J (1993) J Electrochem Soc 140:3114
14. Malinowska B, Cassir M, Delcorso F, Devynck J (1995) J Electroanal Chem 389:21
15. Cassir M, Olivry M, Albin V, Malinowska B, Devynck J (1998) J Electroanal Chem 452:127
16. Chauvaut V, Cassir M, Denos Y (1998) Electrochim Acta 43:1991
17. Chauvaut V, Albin V, Schneider H, Cassir M, Ardelean H, Galtayries A (2000) J Appl Electrochem 30:1405
18. Cassir M, Chauvaut V, Alfarra A, Albin V (2000) J Appl Electrochem 30:1415
19. US Department of Commerce (1986) JANAF thermochemical tables, 3rd edn. US Department of Commerce, Washington
20. Lumsden J (1970) Thermodynamics of molten salt mixtures. Academic Press, New York
21. Barin I (1989) Thermochemical data of pure substances. VCH, Weinheim
22. Marezio M, Remeika JP (1966) J Chem Phys 44:3143
23. Byker HJ, Eliezer I, Nowald RA (1979) J Phys Chem 83:2349
24. Suski L, Tarniowy M (2001) J Mater Sci 36:5119. doi:10.1023/A:1012425324262
25. Danek V, Tarniowy M, Suski L (2004) J Mater Sci 38:2429. doi:10.1023/B:JMSC.0000020006.46296.04